



ARTICLE

## Film Flow of Nano-Micropolar Fluid with Dissipation Effect

Abuzar Abid Siddiqui<sup>1</sup> and Mustafa Turkyilmazoglu<sup>2,3,\*</sup>

<sup>1</sup>Department of Basic Sciences & Humanities, Faculty of Engineering & Technology, Bahauddin Zakariya University, Multan, Pakistan

<sup>2</sup>Department of Mathematics, Hacettepe University, Ankara, Türkiye

<sup>3</sup>Department of Medical Research, China Medical University Hospital, China Medical University, Taichung, Taiwan

\*Corresponding Author: Mustafa Turkyilmazoglu. Email: turkyilm@hacettepe.edu.tr; turkyilm@hotmail.com

Received: 08 February 2024 Accepted: 29 April 2024 Published: 08 July 2024

### ABSTRACT

The physical problem of the thin film flow of a micropolar fluid over a dynamic and inclined substrate under the influence of gravitational and thermal forces in the presence of nanoparticles is formulated. Five different types of nanoparticle samples are accounted for in this current study, namely gold  $Au$ , silver  $Ag$ , molybdenum disulfide  $MoS_2$ , aluminum oxide  $Al_2O_3$ , and silicon dioxide  $SiO_2$ . Blood, a micropolar fluid, serves as the common base fluid. An exact closed-form solution for this problem is derived for the first time in the literature. The results are particularly validated against those for the Newtonian fluid and show excellent agreement. It was found that increasing values of the spin boundary condition and micropolarity lead to a reduction in both the thermal and momentum boundary layers. A quantitative decay in the Nusselt number for a micropolar fluid, as compared to a Newtonian one for all the tested nanoparticles, is anticipated. Gold and silver nanoparticles (i) intensify in the flow parameter as the concentration of nanoparticles increases (ii) yield a higher thermal transfer rate, whereas molybdenum disulfide, aluminum oxide, and silicon dioxide exhibit a converse attitude for both Newtonian and micropolar fluids. The reduction in film thickness for fluid comprising gold particles, as compared to the rest of the nanoparticles, is remarkable.

### KEYWORDS

Thin film flow; micropolar fluid; nanoparticles; molybdenum disulfide; inclined substrate

### Nomenclature

#### Dimensional Quantities

$C_p$	Thermal Capacity ( $JK^{-1}$ )
$g$	Acceleration due to gravity ( $ms^{-2}$ )
$h$	Thickness of the film ( $m$ )
$j_0$	Gyration parameter ( $m^2$ )
$k$	Thermal conductivity ( $Wm^{-1}K^{-1}$ )
$\tilde{p}$	Hydrodynamic pressure ( $kgm^{-1}s^{-2}$ )
$\tilde{S}$	Axial component of spin vector ( $s^{-1}$ )



$T$	Temperature ( $K$ )
$\tilde{u}$	Horizontal component of velocity of fluid ( $ms^{-1}$ )
$\tilde{v}$	Vertical component of velocity of fluid ( $ms^{-1}$ )
$\tilde{x}$	Abscissa ( $m$ )
$\tilde{y}$	Ordinate ( $m$ )
$K_1$	Viscosity parameter
Nu	Nusselt number
$p$	Hydrodynamic pressure
$Q$	Discharge of fluid
Re	Reynolds number
$S$	Axial component of spin vector
$u$	Horizontal component of velocity of fluid
$v$	Vertical component of velocity of fluid
$x$	Abscissa
$y$	Ordinate

### Greek Symbols

$\alpha_1$	Dimensionless flow parameter
$\tilde{\beta}_0$	Dimensionless spin boundary parameter
$\beta_1$	Dimensionless thermal parameter
$\beta_2$	Dimensionless thermal parameter coefficient
$\beta_3$	Dimensionless viscous dissipation parameter
$\chi$	Vorticity Viscosity coefficient ( $kgm^{-1}s^{-1}$ )
$\phi$	Dimensionless Volume fraction
$\gamma$	Spin gradient coefficient ( $kgms^{-1}$ )
$\mu$	Viscosity coefficient ( $kgm^{-1}s^{-1}$ )
$\theta$	Dimensionless temperature
$\theta_c$	Angle of inclination of substrate
$\rho$	Density ( $kgm^{-3}$ )

### Subscripts

f	Fluid
s	Nanoparticles
nf	Nanofluid

## 1 Introduction

### 1.1 Thin Film Flow and Its Significance

Modern Touch of a Classical Flow Problem: Thin films of liquid are pervasive and ubiquitous across both the natural and human-made worlds. Thin film flow describes the spreading of a liquid over a solid substrate (static or dynamic) with a free surface, typically air or gas, at the interface. The flow is primarily driven by external forces, such as a translating or rotating substrate, surface tension, or gravitational force [1,2]. To further explore this, consider examples from nature and technology, including rainwater dribbling down a windowpane, blood coursing through tiny blood vessels, tears trickling down a cheek, suspensions oozing over substrates, and lubricant oil coating rotating ball bearings or other spinning objects [3–6]. Studying thin film flow has wide-ranging applications, aiding

understanding of phenomena such as spin-coating, gravure printing, absorption columns, mudslides, dry processes, cooling of microelectronics devices, production of glass/wire, wettability, flow over roads/roofs, solar cells, film evaporation, food industry processes, and heat exchangers [7–11].

One application of thin film flow studies is the analysis of complex liquid flows over intricate substrates. For example, it can be utilized to model the surface-tension-driven flow of incompressible fluids, such as the lining of the lungs [12,13]. The complexity of these flows arises from two main factors:

- **Substrate geometry:** This can include flexible substrates like leaves [5] or the intricate lining of the lungs [13], as well as other examples like magma streams or tears on a face [14,15].
- **Liquid properties:** Beyond simple Newtonian fluids like pure water, the flow can involve liquids containing mud, non-Newtonian fluids, or even fluids with nanoparticles [16–20]. This study focuses specifically on micropolar fluids, which have complex molecular structures and include examples like blood, liquid crystals, and colloidal suspensions [21,22]. A deeper exploration of the fascinating properties of micropolar fluids will follow.

Currently, many literature sources exist on both theoretical and experimental studies of thin film flow for Newtonian and non-Newtonian fluids.

### *1.2 Literature Survey for Newtonian Fluid*

The story of thin film flow began in 1916 with the work of Nusselt [23], who presented mathematical equations describing its dynamics. He derived the governing equation for thermal transfer coefficients in condensate thin films, assuming they primarily resist heat transfer. Subsequently, a significant contribution was made in 1974 by Tamir et al. [24], who extended Nusselt's work by accounting for a constant surface resistance.

While a full historical account is beyond the scope of this discussion due to its substantial length, several noteworthy contributions have explored various aspects of thin film flow:

- Kondic et al. [25] examined thin film liquid on an inclined plane, concluding that the inclination angle significantly alters the wetting behavior.
- O'Brien et al. [26] built upon this work by detailing the implementation of the thin film lubrication approximation and presenting practical examples.
- Wang et al. [27] investigated the influence of channel shape on condensation in thin films within horizontal microchannels.
- Al-Jarrah et al. [28] described the process of film thickness development in microchannels.
- Gatapova et al. [29] analyzed the thermal effects of thin liquid film flow in a channel heated from below.
- Lin et al. [30] reported the dominant role of convective thermal transfer at high Reynolds numbers.

**Applications and Experimental Verification:** The applications of thin film flow extend beyond theoretical studies. For instance, Mazloomi et al. [31] utilized the lattice-Boltzmann method to investigate thin film flow with thermal sources for surface coating, while Slade [32] explored rivulet formation in thin liquid films. Experimental validation also plays a crucial role in understanding thin film flow. Several studies have focused on this aspect, including:

- Ju et al. [33] performed experiments to probe the droplet impinging on thin film flows and highlighted the characteristics of droplet evolution.

- Charogiannis et al. [34] conducted experiments on thin film flows over inclined glass planes driven by gravity, studying the relationship between the Nusselt number and Reynolds number.
- Wang et al. [35] investigated the thermal influence on thin films under a thermal source environment.
- Budakli [36] experimentally examined thin film flow generated from turbulent gas flow on heated inclined channel walls or under gravitational force.
- Markides et al. [37] conducted experiments to understand the effects of conjugate thermal transfer in thin film flow over electrically heated inclined substrates.

**Micropolar Fluids with Nanoparticles:** It is well known that nanoparticles in liquids can enhance thermal transfer rates and facilitate other valuable industrial phenomena, such as the instant cooling of electronic chips or rapid water heating in geysers and heat exchangers. Notably, reference [10] was the first to theoretically analyze the hydrodynamic and thermal effects of thin film flow in water containing seven different nanoparticles, even developing a closed-form solution for fluid velocity and temperature.

**Contribution and Scope:** Inspired by the work in [10], this study extends its analysis to explore other fluid types, such as micropolar fluids, which are relevant to blood, colloidal suspensions, and epoxies. It derives a closed-form solution for the thin film flow of a micropolar fluid containing five different nanoparticles over a thermally heated inclined plane.

### ***1.3 Literature Survey for Non-Newtonian Fluid***

In various industries, fluids such as tomato ketchup, honey, blood, colloidal suspensions, and mercury, along with other industrial fluids, do not behave ideally like water. These liquids are categorized as non-Newtonian fluids and require distinct models and constitutive equations to describe their flow behavior. The study of the thin film flow of such non-Newtonian fluids has yielded valuable insights [38–42]. To further explore it, let us examine some recent contributions from 2021 to 2023.

**Recent Highlights (2021–2023):**

- 2021:
  - Reference [43]: This study compared two methods, homotopy perturbation Elzaki transform and Elzaki decomposition, for analyzing the thin film flow of a third-grade fluid down an inclined plane, favoring the former for its efficacy.
  - Reference [44]: Research on Oldroyd-B ferrofluid containing nanoparticles (Cobalt Ferrite) employed the Runge-Kutta method for a numerical solution.
- 2022:
  - Reference [45]: Thin film flow of a Williamson fluid was numerically investigated using a homotopy-based scheme with Fractional Calculus, considering bio-convection and microorganism diffusivity.
  - Reference [46]: This study explored the thin film flow of a Casson nanofluid.
  - Reference [47]: This study analyzed viscoplastic Bingham fluid's thin film flow behavior.
  - Reference [48]: Johnson-Segalman fluid was the focus of this study on thin film flow.
- 2023:
  - Reference [49]: A third-grade fluid's thin film flow characteristics were investigated.
  - Reference [50]: Johnson-Segalman fluid was tackled in this study on thin film flow.

- Reference [51]: Second-grade fluid's thin film flow behavior was analyzed.
- Reference [52]: Maxwell nanofluid's thin film flow was explored.
- Reference [53]: This study focused on Casson nanofluid, further advancing the understanding of thin film flow behavior.

Looking Forward: These examples highlight the active research landscape in non-Newtonian thin film flows. As this field continues to evolve, it offers immense potential for advancements in diverse areas such as bioengineering, microfluidics, and coating technologies.

#### **1.4 Current Study and Micropolar Fluid**

As discussed earlier, this study focuses on exploring the hydro- and thermo-dynamical effects of thin film flow in micropolar fluids containing nanoparticles. These fluids hold significant technological value and exist not only in the laboratory but also in the natural world. Blood, which represents the micropolar nature with its cellular and platelet components, is noted in [54,55]. Colloidal suspensions and liquid crystals, characterized by the presence of colloids, are also part of this category [56]. Rigid-rod epoxies, with their rod-like molecular structure and polymeric suspensions, further expand the diverse scope of micropolar fluids [22,57].

Micropolar fluids are distinguished from Newtonian and non-Newtonian fluids through their ability to sustain body couple and couple stress in addition to conventional body force and Cauchy stress. The Cauchy stress tensor in a micropolar fluid arises from the microscopic, needle-like particles it contains. While Newtonian fluids require only three degrees of freedom for analysis, micropolar fluids necessitate six, reflecting their more complex internal structure.

The literature on the thin film flow of micropolar fluids remains surprisingly sparse. A notable study from Yusuf et al. in 2021 [58] investigated this phenomenon over a static inclined porous substrate, primarily focusing on entropy analysis and employing numerical tools based on the differential transformation method. While this study is noteworthy, it leaves several intriguing questions unanswered, thus hindering a comprehensive understanding of micropolar fluid behavior in real-world situations.

Unanswered Questions and the Research Focus: These unaddressed questions become the driving force for the present research. For instance, how will the fluid respond to a heater within or near the substrate? What happens when the substrate becomes dynamic, moving at a uniform or non-uniform speed? What impact do different nanoparticles, incorporated as additive colloids, have on the flow dynamics? These and many more questions will guide this research, promising valuable insights into the world of micropolar fluids.

The Power of Nanoparticles: Nanoparticles play a vital role in shaping the landscape of modern technology [59–62]. Gold (Au) and silver (Ag) nanoparticles are extensively used in separation science, facilitating efficient separation processes [63–65]. Solutions of gold nanoparticles even reduce thermal resistance by 13% compared to pure water. These nanoparticles also hold vast potential in cancer treatment, where their heat-generating capability aids in photodynamic therapy.

Molybdenum disulfide  $MoS_2$  shines in the field of electronics and logic devices due to its tunable semi-conductive properties. It also serves as a solid lubricant additive in greases and gear oils, enhancing their performance by reducing friction and wear, lowering operating temperatures, and increasing load-carrying capacity. Additionally,  $MoS_2$  helps dampen vibration and noise, leading to reduced energy consumption. Its antioxidant and anti-corrosion properties further contribute to extending the life of lubricants [66–68].

Aluminum oxide ( $Al_2O_3$ ) nanoparticles are prominent in the medical field as antibacterial agents owing to their low toxicity towards eukaryotic cells [69]. Silicon dioxide ( $SiO_2$ ) nanoparticles, on the other hand, improve combustion efficiency and reduce emissions in dual-fuel engines.  $SiO_2$ -based nanofluids, particularly those in methanol, can increase peak heat release rate and peak pressure by up to 4.3% and 8.6%, respectively, while also enhancing brake-specific fuel consumption and brake thermal efficiency under high loads [70,71].

**The Current Study:** This study explores the thin film flow of a micropolar fluid (base fluid) containing five distinct types of nanoparticles. This flow occurs over an inclined substrate moving with a uniform speed ( $U$ ) under the influence of gravity. Section 2 meticulously formulates the governing equations for this scenario. Section 3 then tackles the derivation of a closed-form exact solution for the corresponding boundary value problem. Section 4 shows the obtained results and provides insightful commentary on their implications. Finally, Section 5 wraps up the study by summarizing the essential findings and their significance.

## 2 Mathematical Formulation and Analysis of the Physical Problem

The governing equations for a steady flow of an incompressible, two-dimensional nano-micropolar fluid model [10,22,56] in the presence of viscous dissipation and in the absence of Joule heating and electromagnetic influences can be written as follows:

$$\frac{\partial \tilde{u}}{\partial \tilde{x}} + \frac{\partial \tilde{v}}{\partial \tilde{y}} = 0 \quad (1)$$

$$\tilde{u} \frac{\partial \tilde{u}}{\partial \tilde{x}} + \tilde{v} \frac{\partial \tilde{u}}{\partial \tilde{y}} = -g \sin \theta_c - \frac{1}{\rho_{nf}} \frac{\partial \tilde{p}}{\partial \tilde{x}} + \frac{(\mu_{nf} + \chi)}{\rho_{nf}} \left[ \frac{\partial^2 \tilde{u}}{\partial \tilde{x}^2} + \frac{\partial^2 \tilde{u}}{\partial \tilde{y}^2} \right] + \frac{\chi}{\rho_{nf}} \frac{\partial \tilde{S}}{\partial \tilde{y}} \quad (2)$$

$$\tilde{u} \frac{\partial \tilde{v}}{\partial \tilde{x}} + \tilde{v} \frac{\partial \tilde{v}}{\partial \tilde{y}} = -g \cos \theta_c - \frac{1}{\rho_{nf}} \frac{\partial \tilde{p}}{\partial \tilde{y}} + \frac{(\mu_{nf} + \chi)}{\rho_{nf}} \left[ \frac{\partial^2 \tilde{v}}{\partial \tilde{x}^2} + \frac{\partial^2 \tilde{v}}{\partial \tilde{y}^2} \right] + \frac{\chi}{\rho_{nf}} \frac{\partial \tilde{S}}{\partial \tilde{x}} \quad (3)$$

$$\tilde{u} \frac{\partial \tilde{S}}{\partial \tilde{x}} + \tilde{v} \frac{\partial \tilde{S}}{\partial \tilde{y}} = \frac{\gamma}{j_0 \rho_{nf}} \left[ \frac{\partial^2 \tilde{S}}{\partial \tilde{x}^2} + \frac{\partial^2 \tilde{S}}{\partial \tilde{y}^2} \right] + \frac{\chi}{j_0 \rho_{nf}} \left[ \frac{\partial \tilde{v}}{\partial \tilde{x}} - \frac{\partial \tilde{u}}{\partial \tilde{y}} - 2\tilde{S} \right] \quad (4)$$

$$(\rho C_p)_{nf} \left[ \tilde{u} \frac{\partial T}{\partial \tilde{x}} + \tilde{v} \frac{\partial T}{\partial \tilde{y}} \right] = k_{nf} \left[ \frac{\partial^2 T}{\partial \tilde{x}^2} + \frac{\partial^2 T}{\partial \tilde{y}^2} \right] + \mu_{nf} \left[ \left( \frac{\partial \tilde{v}}{\partial \tilde{x}} + \frac{\partial \tilde{u}}{\partial \tilde{y}} \right)^2 + 2 \left( \frac{\partial \tilde{u}}{\partial \tilde{x}} \right)^2 + 2 \left( \frac{\partial \tilde{v}}{\partial \tilde{y}} \right)^2 \right] \quad (5)$$

where  $(\tilde{u}, \tilde{v})$  represents dimensional velocity components along  $(\tilde{x}, \tilde{y})$  directions;  $\tilde{p}$  is the dimensional pressure;  $\tilde{S}$  is axial component of the dimensional micro-rotation (spin) vector;  $j_0$  is the micro-inertia or gyration parameter;  $\gamma$  is the spin-gradient coefficient. The density, thermal conductivity, and viscosity coefficient of liquid comprising nanoparticles are correlated as follows:

$$\rho_{nf} = (1 - \varphi) \rho_f + \varphi \rho_s \quad (6a)$$

$$k_{nf} = k_f \frac{k_s + 2k_f - 2\varphi(k_f - k_s)}{k_s + 2k_f + \varphi(k_f - k_s)} \quad (6b)$$

$$\text{and } \mu_{nf} = (1 - \varphi)^{-2.5} \mu_f \quad (6c)$$

where  $\varphi$  is the volume fraction or concentration of nanoparticles, whereas the subscripts  $f$  and  $s$  represent fluid and nanoparticle, respectively;  $\chi$  is the vortex viscosity coefficient such that  $\chi + 2\mu \geq 0$  where  $\chi \geq 0$  [56]. It is important to note that  $\chi$  will be zero for a Newtonian fluid.

The above equations can be written in dimensionless form as follows:

$$\frac{\partial u}{\partial x} + \frac{\partial v}{\partial y} = 0 \tag{7}$$

$$\text{Re} \left[ u \frac{\partial u}{\partial x} + v \frac{\partial u}{\partial y} \right] = -\gamma_1 \sin \theta_c - \text{Re} \frac{\partial p}{\partial x} + \nabla^2 u + K_1 \frac{\partial S}{\partial y} \tag{8}$$

$$\text{Re} \left[ u \frac{\partial v}{\partial x} + v \frac{\partial v}{\partial y} \right] = -\gamma_1 \cos \theta_c - \text{Re} \frac{\partial p}{\partial y} + \nabla^2 v + K_1 \frac{\partial S}{\partial x} \tag{9}$$

$$K_3 \left[ u \frac{\partial S}{\partial x} + v \frac{\partial S}{\partial y} \right] = \nabla^2 S + K_2 \left[ \frac{\partial v}{\partial x} - \frac{\partial u}{\partial y} - 2S \right] \tag{10}$$

and

$$\beta_2 \left[ u \frac{\partial \theta}{\partial x} + v \frac{\partial \theta}{\partial y} \right] = \nabla^2 \theta + \beta_3 \left[ \left( \frac{\partial v}{\partial x} + \frac{\partial u}{\partial y} \right)^2 + 2 \left( \frac{\partial u}{\partial x} \right)^2 + 2 \left( \frac{\partial v}{\partial y} \right)^2 \right] \tag{11}$$

by balancing  $(u, v) = (\tilde{u}, \tilde{v})/U$ ,  $(x, y) = (\tilde{x}, \tilde{y})/h$ ,  $p = \tilde{p}/U^2 \rho_{nf}$ ,  $S = h\tilde{S}/U$  and  $\theta = (T - T_0)/\Delta T$ . Here  $\Delta T$  is the temperature difference between the temperature of ambient flow and that of the wall  $T_0$ ;  $\nabla^2$  is the two-dimensional Laplacian operator.

$$\text{Re} = \frac{Uh\rho_{nf}}{(\mu_{nf} + \chi)}, \gamma_1 = \frac{h^2\rho_{nf}}{(\mu_{nf} + \chi)U}, K_1 = \frac{\chi}{(\mu_{nf} + \chi)}, k_2 = \frac{\chi h^2}{\gamma}, \text{ and } k_3 = \frac{j_0 h U \rho_{nf}}{\gamma} \tag{12}$$

This study considers the nano-micropolar liquid flowing over an inclined substrate with an angle of inclination, as shown in Fig. 1.

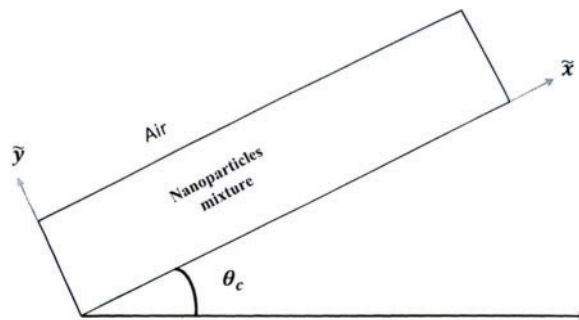


**Figure 1:** Flow configuration

The flow is generated by a pulling roller that is sliding along the x-axis with a constant fluid speed  $U$ . Additionally, it is assumed that the thickness ( $h$ ) of the liquid film is less than the boundary layer thickness. Furthermore, the shear stress exerted by the air on the air-liquid interface is neglected, which will facilitate mathematical calculations. However, due to the influence of gravity ( $g$ ), the thickness of the liquid representing the air-liquid interface may not remain uniform, and reverse flow may occur. These effects are considered infinitesimal influences on the ambient flow by compensating for the pulling speed of the liquid-carrier film [10]. The liquid considered has specific characteristics: its molecules are either rod- or dumbbell-shaped, exhibiting microrotation and couple stress in addition to usual stress. Such a liquid is typically referred to as a Cosserat or micropolar fluid [56]. Nanoparticles are added to the base liquid, the micropolar liquid, to enhance the thermal transfer rate. Five different

types of nanoparticles are used as a test sample. It is assumed that the nanoparticles remain stable during fluid flow. The thermodynamical properties of these elements/compounds are presented in Table 1. Moreover, it is assumed that the liquid film, adhering to the x-axis, is uniformly heated and maintains a temperature of  $T_0$  at all times and points of the film. The thermal flux at the air-liquid interface is assumed to be zero [10].

**Table 1:** Physical properties of nanoparticles and base fluids at 20°C [10,72,73]

Fluid/Nanoparticles	$C_p$ (J/Kg. K)	$k$ (J/m.sec.K)	$\rho$ (Kg/m <sup>3</sup> )
Water	4179	0.613	997.1
Blood	3617	0.49	1060
Gold $Au$	129	318	19300
Silver $Ag$	235	429	10500
Molybdenum disulfide $MoS_2$	397.21	100	5060
Aluminum oxide $Al_2O_3$	765	40	3970
Silicon dioxide $SiO_2$	703	1.38	2200

Based on the aforementioned assumptions, Eqs. (8)–(11) deform, ensuring that Eq. (7) is satisfied as follows:

$$\frac{d^2u}{dy^2} + K_1 \frac{dS}{dy} = \alpha_1 \quad (13)$$

$$Re \frac{dp}{dy} = \gamma_1 \cos \theta_c \quad (14)$$

$$\frac{d^2S}{dy^2} - 2K_2S = K_2 \frac{du}{dy}, \quad (15)$$

$$\text{and } \frac{\partial^2 \theta}{\partial y^2} = \beta_1 u - \beta_3 \left( \frac{du}{dy} \right)^2 \quad (16)$$

$$\text{where } \alpha_1 = \gamma_1 \sin \theta_c, \quad (17a)$$

$$\text{and } \beta_1 = \beta_2 \frac{\partial \theta}{\partial x} = \text{constant}. \quad (17b)$$

Furthermore, the boundary conditions can be written as follows:

$$u = 1, \theta = 0, S = \beta_0 \left( \frac{du}{dy} \right)_{y=0} = \tilde{\beta}_0 \text{ at } y = 0 \quad (18a)$$

$$\frac{du}{dy} = 0, \frac{\partial \theta}{\partial y} = 0, S = 0 \text{ at } y = 1 \quad (18b)$$

$$u = 1, \theta = 0, S = \beta_0 \left( \frac{du}{dy} \right)_{y=0} = \tilde{\beta}_0 \text{ at } y = 0 \quad (18c)$$

$$\frac{du}{dy} = 0, \frac{\partial \theta}{\partial y} = 0, S = 0 \text{ at } y = 1 \quad (18d)$$

### 3 Analytical Solution of the Problem

The aforementioned BVP in Eqs. (13)–(17) contains linear coupled ODE. Hence, it can be integrated exactly using standard methods. The solution for the fluid speed  $u(y)$ , spin  $S(y)$ , and temperature  $\theta(y)$  are summarized as follows:

$$u(y) = 1 - \frac{K_1 A_2}{\lambda_1} [-1 - e^{2\lambda_1} + e^{\lambda_1 y} + e^{2\lambda_1 - \lambda_1 y}] + A_3 \left[ \frac{y^2}{2} - y \right] \tag{19}$$

$$S(y) = A_2 [e^{\lambda_1 y} - e^{2\lambda_2 - \lambda_1 y}] - \frac{\alpha_1}{2 - K_1} [y - 1], \tag{20}$$

$$\begin{aligned} \text{and } \theta(y) = & \beta_1 \left\{ -y + \frac{y^2}{2} + A_3 \left[ \frac{y}{3} - \frac{y^3}{6} + \frac{y^4}{24} \right] \right\} + \frac{A_2 K_1 \beta_1}{\lambda_1^2} \left\{ 2e^{\lambda_1} - \frac{e^{2y\lambda_1}}{2} \right\} y \\ & + \frac{1}{\lambda_1} \left\{ \left[ (e^{2\lambda_1} - 1)y + \frac{y^2}{2} \right] A_2 K_1 \beta_1 + [-1 - e^{4\lambda_1} + e^{2y\lambda_1} + e^{2\lambda_1(2-y)}] \frac{A_2^2 K_1^2 \beta_3}{2} \right\} \\ & + \beta_3 \left\{ \left[ -\frac{y}{3} + \frac{y^2}{2} + \frac{y^3}{3} + \frac{y^4}{12} \right] A_3^2 + [2 - y] y e^{2\lambda_1} A_2^2 K_1^2 \right\} \\ & + \frac{A_2 K_1 \beta_1}{\lambda_1^3} \left\{ \frac{3}{4} - e^{2\lambda_1} - e^{y\lambda_1} + \frac{e^{2y\lambda_1}}{4} + e^{(2-y)\lambda_1} \right\} \\ & + \frac{4A_2 A_3 K_1 \beta_3 e^{2\lambda_1}}{\lambda_1^3} \{ \cosh[\lambda_1] - \cosh[(y - 1)\lambda_1] \} \\ & + \frac{2A_2 A_3 K_1 \beta_3 e^{2\lambda_1}}{\lambda_1^2} \{ \sinh[\lambda_1] - (y - 1) \sinh[(y - 1)\lambda_1] \} \end{aligned} \tag{21}$$

In this scenario, the expression for thermal flux is as follows:

$$\begin{aligned} \frac{d}{dy} \theta(y) = & \beta_1 \left\{ -1 + y + A_3 \left[ \frac{1}{3} - \frac{y^2}{2} + \frac{y^3}{64} \right] \right\} + \frac{A_2 K_1 \beta_1}{\lambda_1^2} \left\{ 2e^{\lambda_1} - \frac{1}{2} [2\lambda_1 y + 1] e^{2y\lambda_1} \right\} \\ & + \frac{1}{\lambda_1} \left\{ [e^{2\lambda_1} - 1 + y] A_2 K_1 \beta_1 + [2\lambda_1 e^{2y\lambda_1} + 2\lambda_1 e^{2\lambda_1(2-y)}] \frac{A_2^2 K_1^2 \beta_3}{2} \right\} \\ & + \beta_3 \left\{ \left[ -\frac{1}{3} + y + y^2 + \frac{y^3}{3} \right] A_3^2 + [1 - y] 2e^{2\lambda_1} A_2^2 K_1^2 \right\} \\ & + \frac{A_2 K_1 \beta_1}{\lambda_1^2} \left\{ -e^{y\lambda_1} + \frac{e^{2y\lambda_1}}{2} - e^{(2-y)\lambda_1} \right\} + \frac{4A_2 A_3 K_1 \beta_3 e^{2\lambda_1}}{\lambda_1^2} \{ \sinh[(y - 1)\lambda_1] \} \\ & + \frac{2A_2 A_3 K_1 \beta_3 e^{2\lambda_1}}{\lambda_1^2} \{ -\sinh[(y - 1)\lambda_1] - \lambda_1 (y - 1) \cosh[(y - 1)\lambda_1] \} \end{aligned} \tag{22}$$

where

$$A_2 = \left( -\tilde{\beta}_0 + \alpha_1/2 - K_1 \right) / (e^{2\lambda_1} - 1); A_3 = 2\alpha_1 / (2 - K_1); \lambda_1 = \sqrt{(2 - K_1) K_2}. \tag{23}$$

If  $K_1 = 0$  and  $\beta_3 = 0$ , then Eqs. (19)–(21) can be reduced to the speed, temperature, and thermal flux for the Newtonian fluid [10].

## 4 Results and Discussion

This section is devoted to presenting some dominant results both in tabular and pictorial forms and commenting on them. The results are based on the exact closed-form solution, Eqs. (19)–(21), of the physical problem under consideration.

### 4.1 Fluid Speed

In order to validate the calculations herein, Fig. 2b is set for fluid speed if  $K_1 = 0$  in Eq. (19) particularly for the Newtonian fluid. This figure agrees well with Fig. 2b of [10]. This satisfaction provided motivation to study the fluid speed for  $K_1 \neq 0$ , micropolar fluid, which is shown in Fig. 2a for different values of flow parameter  $\alpha_1$ .

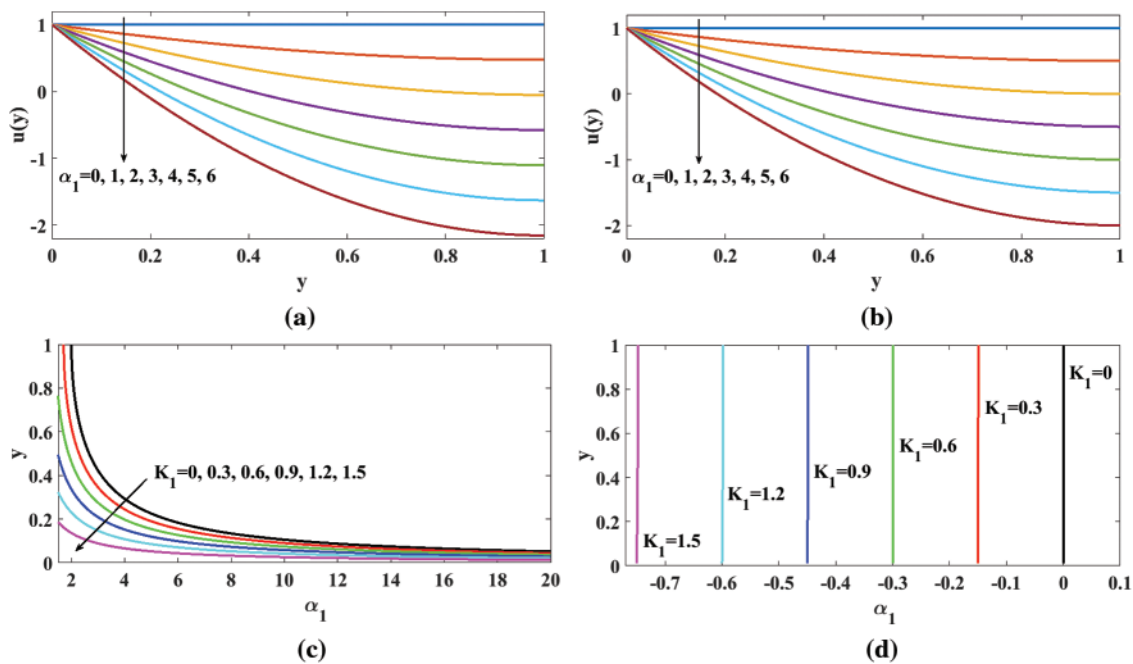


**Figure 2:** Fluid-speed profiles for: (a) micropolar fluid; (b) Newtonian fluid for different values of  $\alpha_1$  when  $K_1 = 0.5$  with no-spin boundary condition;  $\tilde{\beta}_0 = 0$ ; (c) stagnation point study of the speed of fluid; (d) separation point study of speed of fluid

As the flow is generated by moving upward the inclined substrate over it, the fluid is flowing, and the probability of reverse flow downward naturally is dominant. This fact is reflected in Fig. 2a as a negation of speed substrate-rider fluid. This reversal of fluid dominates with the rise in the flow parameter  $\alpha_1$ . This phenomenon aligns with the physical situation because  $\alpha_1$  is linearly proportional to the angle of inclination  $\theta_c$  of substrate by virtue of Eq. (17a). However, the critical points at which the reverse flow takes place rely on various factors, in which one of the factors is flow parameter  $\alpha_1$ . The range of flow parameter is  $\alpha_1 \in [0, 2)$  for which rider fluid-film moves with the moving substrate for both the Newtonian fluid ( $K_1 = 0$ ) as well as the micropolar fluid ( $K_1 \neq 0$ ). Nevertheless, the speed of reverse flow increases for the micropolar fluid, which is not surprising because the effects of micropolarity are enhanced, as shown in Figs. 2a and 2b. The threshold value  $\alpha_1 = 2$  is common for both the Newtonian fluid ( $K_1 = 0$ ) and the micropolar fluid ( $K_1 \neq 0$ ) at which the reverse flow initiates caused by the gravitational force, provided that a no-spin boundary condition  $\tilde{\beta}_0 = 0$  is imposed. When

a spin boundary condition  $\tilde{\beta}_0 \neq 0$  is encountered, then the threshold value of  $\alpha_1$  varies such that  $\alpha_1 = 1$  if  $\tilde{\beta}_0 = 0.6$ , as shown in Fig. 3. Additionally, the following facts for the flow attitude are also observed based on Eq. (18) generally and particularly in Table 2.

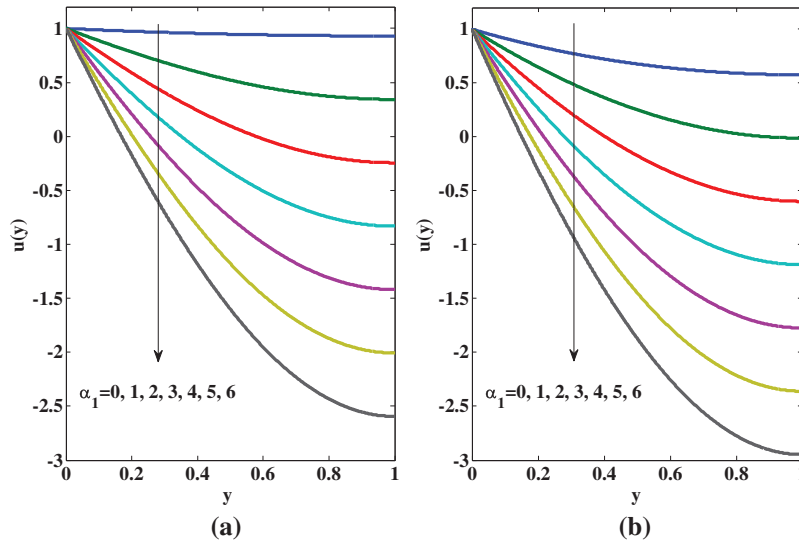


**Figure 3:** The effect of spin boundary condition on the fluid speed for micropolar fluid for different values of  $\alpha_1$  when  $K_1 = 1.5$  if spin coefficient: (a)  $\tilde{\beta}_0 = 0.1$ ; (b)  $\tilde{\beta}_0 = 0.6$

**Table 2:** Derived expressions for fluid speed, discharge, temperature, and thermal flux at the boundaries of the substrate

$K_1$	$\beta_3$	$\tilde{\beta}_0$	$u(1)$	$u'(0)$	$Q$	$\theta(1)$	$\theta'(0)$
$\neq 0$	$\neq 0$	$\neq 0$	$u_1$	$-\alpha_1 - K_1 \tilde{\beta}_0$	$1 + \frac{K_1 \tilde{\beta}_0 (1 - \text{Coth}[\lambda_1] \lambda_1)}{\lambda_1^2} + \frac{\alpha_1 (2\lambda_1^2 + K_1 (3 - 3\text{Coth}[\lambda_1] \lambda_1))}{3(-2 + K_1) \lambda_1^2}$	$\frac{T_1 + \tilde{\beta}_0 T_2}{(K_1 - 2)^2}$	$\frac{F_1 + \tilde{\beta}_0 F_3}{(K_1 - 2)^2}$
$\neq 0$	$\neq 0$	$= 0$	$u_2$	$-\alpha_1$	$1 + \frac{\alpha_1 (2\lambda_1^2 + K_1 (3 - 3\text{Coth}[\lambda_1] \lambda_1))}{3(-2 + K_1) \lambda_1^2}$	$\frac{T_1}{(K_1 - 2)^2}$	$\frac{F_1}{(K_1 - 2)^2}$
$\neq 0$	$= 0$	$\neq 0$	$u_1$	$-\alpha_1 - K_1 \tilde{\beta}_0$	$1 + \frac{K_1 \tilde{\beta}_0 (1 - \text{Coth}[\lambda_1] \lambda_1)}{\lambda_1^2} + \frac{\alpha_1 (2\lambda_1^2 + K_1 (3 - 3\text{Coth}[\lambda_1] \lambda_1))}{3(-2 + K_1) \lambda_1^2}$	$\frac{T_3 + \tilde{\beta}_0 T_4}{(K_1 - 2)^2}$	$\frac{F_2 + \tilde{\beta}_0 F_4}{K_1 - 2}$
$\neq 0$	$= 0$	$= 0$	$u_1$	$-\alpha_1$	$1 + \frac{\alpha_1 (2\lambda_1^2 + K_1 (3 - 3\text{Coth}[\lambda_1] \lambda_1))}{3(-2 + K_1) \lambda_1^2}$	$\frac{T_3}{(K_1 - 2)^2}$	$\frac{F_2}{K_1 - 2}$
$= 0$	$\neq 0$	$\neq 0$	$1 - \frac{\alpha_1}{2}$	$-\alpha_1$	$1 - \frac{\alpha_1}{3}$	$-\frac{\beta_1}{2} + \frac{5\alpha_1 \beta_1}{24}$	$-\frac{\beta_1}{3} + \frac{\alpha_1 \beta_1}{3}$
						$-\frac{1}{12} \alpha_1^2 \beta_3$	$-\frac{1}{3} \alpha_1^2 \beta_3$

(Continued)

**Table 2 (continued)**

$K_1$	$\beta_3$	$\tilde{\beta}_0$	$u(1)$	$u'(0)$	$Q$	$\theta(1)$	$\theta'(0)$
$= 0$	$\neq 0$	$= 0$	$1 - \frac{\alpha_1}{2}$	$-\alpha_1$	$1 - \frac{\alpha_1}{3}$	$-\frac{\beta_1}{2} + \frac{5\alpha_1\beta_1}{24}$	$-\frac{\beta_1}{3} + \frac{\alpha_1\beta_1}{3}$
$= 0$	$= 0$	$\neq 0$	$1 - \frac{\alpha_1}{2}$	$-\alpha_1$	$1 - \frac{\alpha_1}{3}$	$-\frac{1}{12}\alpha_1^2\beta_3$	$-\frac{1}{3}\alpha_1^2\beta_3$
$= 0$	$= 0$	$= 0$	$1 - \frac{\alpha_1}{2}$	$-\alpha_1$	$1 - \frac{\alpha_1}{3}$	$-\frac{\beta_1}{2} + \frac{5\alpha_1\beta_1}{24}$	$-\frac{\beta_1}{3} + \frac{\alpha_1\beta_1}{3}$

where

$$u_1 = u_2 + \frac{K_1\tilde{\beta}_0}{\lambda_1(e^{\lambda_1} + 1)} \tag{24}$$

$$u_2 = 1 + \frac{\alpha_1}{K_1 - 2} + \frac{K_1\alpha_1(e^{\lambda_1} - 1)}{\lambda_1(e^{\lambda_1} + 1)(K_1 - 2)} \tag{25}$$

$$T_1 = \beta_1 \left[ 2 + 2K_1 - \frac{K_1^2}{2} + \frac{5}{6}\alpha_1 - 5K_1\alpha_1 \right] + \frac{\alpha_1\beta_3}{\text{Sinh}^2(\lambda_1)} \left[ -\frac{\alpha_1\text{Sinh}^2(\lambda_1)}{3} + \frac{K_1^2\alpha_1}{4} \right] \tag{26}$$

$$+ \frac{3K_1\alpha_1[K_1 - 2]}{4} + \frac{4\alpha_1^2\beta_3K_1e^{2\lambda_1}}{\lambda_1^3} [1 - \text{Cosh}(\lambda_1) - \text{Coth}(\lambda_1) + \text{Cosh}(\lambda_1)\text{Coth}(\lambda_1)]$$

$$+ \frac{\alpha_1\beta_1K_1}{\lambda_1^2} \left[ -\frac{1}{2} - \frac{\text{Coth}(\lambda_1)}{2} + \frac{2}{\text{Sinh}(\lambda_1)} + \frac{K_1}{4} + \frac{K_1\text{Coth}(\lambda_1)}{4} - \frac{K_1}{\text{Sinh}(\lambda_1)} \right]$$

$$+ \frac{2\alpha_1^2\beta_3K_1e^{2\lambda_1}}{\lambda_1^2} [\text{Sinh}(\lambda_1) - \text{Cosh}(\lambda_1)] + \frac{\alpha_1\beta_1K_1}{\lambda_1} \left[ \frac{3}{2} + \frac{\text{Coth}(\lambda_1)}{2} - \frac{3K_1}{4} - \frac{K_1\text{Coth}(\lambda_1)}{4} \right]$$

$$T_2 = K_1^2\alpha_1\beta_3 \left[ -1 + \frac{K_1}{2} + \tilde{\beta}_0 - K_1\tilde{\beta}_0 + K_1^2\tilde{\beta}_0 \right] + \frac{3\beta_1K_1}{\lambda_1^3} \left[ 1 - K_1 + \frac{K_1^2}{4} \right] - \frac{\alpha_1\beta_3K_1[K_1 - 2]}{\lambda_1}$$

$$- \frac{K_1^2\tilde{\beta}_0\beta_3}{2\lambda_1} [4 - 4K_1 + K_1^2]$$

$$+ \frac{8\alpha_1\beta_3K_1e^{2\lambda_1}}{2\lambda_1^3} [K_1 - 2] [-1 + \text{Cosh}(\lambda_1) + \text{Coth}(\lambda_1) - \text{Cosh}(\lambda_1)\text{Coth}(\lambda_1)]$$

$$\begin{aligned}
 & + \frac{\beta_1 K_1}{4\lambda_1^2} [4 - 4K_1 + K_1^2] \left[ 1 + \text{Coth}(\lambda_1) - \frac{4}{\text{Sinh}(\lambda_1)} \right] \\
 & - \frac{2\alpha_1 \beta_3 K_1 e^{2\lambda_1}}{\lambda_1^2} [(K_1 + 2) \text{Sinh}(\lambda_1) - (K_1 - 2) \text{Cosh}(\lambda_1)] \\
 & + \frac{\beta_1 K_1}{\lambda_1} \left[ -3 - \text{Coth}(\lambda_1) + 3K_1 + K_1 \text{Coth}(\lambda_1) - \frac{3}{4} K_1^2 - \frac{K_1^2 \text{Coth}(\lambda_1)}{4} \right]
 \end{aligned} \tag{27}$$

$$\begin{aligned}
 T_3 = & \beta_1 \left[ 2 + 2K_1 - \frac{K_1^2}{2} + \frac{5}{6} \alpha_1 - 5K_1 \alpha_1 \right] + \frac{3\alpha_1 \beta_1 K_1}{4\lambda_1^3} [K_1 - 2] \\
 & + \frac{\alpha_1 \beta_1 K_1}{\lambda_1} \left[ \frac{3}{2} + \frac{\text{Coth}(\lambda_1)}{2} - \frac{3K_1}{4} - \frac{K_1 \text{Coth}(\lambda_1)}{4} \right] \\
 & + \frac{\alpha_1 \beta_1 K_1}{\lambda_1^2} \left[ -\frac{1}{2} - \frac{\text{Coth}(\lambda_1)}{2} + \frac{2}{\text{Sinh}(\lambda_1)} + \frac{K_1}{4} + \frac{K_1 \text{Coth}(\lambda_1)}{4} - \frac{K_1}{\text{Sinh}(\lambda_1)} \right]
 \end{aligned} \tag{28}$$

$$\begin{aligned}
 T_4 = & \frac{3\beta_1 K_1}{\lambda_1^3} \left[ 1 - K_1 + \frac{K_1^2}{4} \right] + \frac{\beta_1 K_1}{4\lambda_1^2} [4 - 4K_1 + K_1^2] \left[ 1 + \text{Coth}(\lambda_1) - \frac{4}{\text{Sinh}(\lambda_1)} \right] \\
 & + \frac{\beta_1 K_1}{\lambda_1} \left[ -3 - \text{Coth}(\lambda_1) + 3K_1 + K_1 \text{Coth}(\lambda_1) - \frac{3}{4} K_1^2 - \frac{K_1^2 \text{Coth}(\lambda_1)}{4} \right] \\
 & + \frac{\beta_1 K_1}{\lambda_1} \left[ -3 - \text{Coth}(\lambda_1) + 3K_1 + K_1 \text{Coth}(\lambda_1) - \frac{3}{4} K_1^2 - \frac{K_1^2 \text{Coth}(\lambda_1)}{4} \right]
 \end{aligned} \tag{29}$$

$$\begin{aligned}
 F_1 = & \beta_1 \left[ -4 + 4K_1 - K_1^2 + \frac{4}{3} \alpha_1 - \frac{2}{3} K_1 \alpha_1 \right] + \alpha_1^2 \beta_3 \left[ -\frac{4}{3} + \frac{K_1^2 (1 - \text{Sinh}(2\lambda_1))}{2\text{Sinh}^2(\lambda_1)} \right] \\
 & + \frac{\alpha_1 \beta_1 K_1}{\lambda_1} [2 - K_1] \\
 & - \frac{2\alpha_1^2 \beta_3 K_1 \text{Cosh}(\lambda_1)}{\lambda_1} [1 + \text{Coth}(\lambda_1)] + \frac{\alpha_1 \beta_1 K_1 \text{Tanh}(\lambda_1)}{\lambda_1^2} [K_1 - 2] + \frac{2\alpha_1^2 \beta_3 K_1 e^{\lambda_1}}{\lambda_1^2}
 \end{aligned} \tag{30}$$

$$F_2 = \beta_1 \left\{ 2 - K_1 - \frac{2}{3} \alpha_1 + \frac{K_1 \alpha_1}{\lambda_1^2} \left[ -\lambda_1 + \text{Tanh}\left(\frac{\lambda_1}{2}\right) \right] \right\} \tag{31}$$

$$\begin{aligned}
 F_3 = & \frac{\alpha_1 \beta_3 K_1^2}{\text{Sinh}^2(\lambda_1)} [1 - \text{Sinh}(2\lambda_1)] [K_1 - 2] + \left[ -\frac{\beta_1 K_1}{\lambda_1^2} + \frac{\beta_1 K_1 \text{Tanh}\left(\frac{\lambda_1}{2}\right)}{\lambda_1^2} \right] [4 - 4K_1 + K_1^2] \\
 & - \frac{2\alpha_1^2 \beta_3 K_1 \text{Cosh}(\lambda_1)}{\lambda_1} [1 + \text{Coth}(\lambda_1)] + \tilde{\beta}_0 \frac{2\beta_3 K_1^2}{\text{Sinh}^2(\lambda_1)} [4 - 4K_1 + K_1^2] [1 - \text{Sinh}(2\lambda_1)] \\
 & + \tilde{\beta}_0 \frac{2\beta_3 K_1^2}{\text{Sinh}^2(\lambda_1)} [4 - 4K_1 + K_1^2] [1 - \text{Sinh}(2\lambda_1)]
 \end{aligned} \tag{32}$$

$$F_4 = \frac{K_1 \alpha_1 \beta_1}{\lambda_1^2} \left[ -\lambda_1 + \text{Tanh}\left(\frac{\lambda_1}{2}\right) \right] [K_1 - 2] \tag{33}$$

(i) For the Newtonian fluid ( $K_1 = 0$ ), Eq. (19) reduces to

$$u = 1 + \alpha_1 (0.5y^2 - y), \tag{34}$$

It coincides with [10], as attempted for the Newtonian fluid. Further if angle of inclination is zero that implies  $\alpha_1 = 0$  then Eqs. (19) and (34) yield

$$u = \begin{cases} 1 & \text{if } \tilde{\beta}_0 = 0 \\ 1 - \frac{\tilde{\beta}_0 K_1}{\lambda_1 (e^{2\lambda_1} - 1)} [e^{2\lambda_1 - \lambda_1 y} + e^{\lambda_1 y} - e^{2\lambda_1} - 1] & \text{if } \tilde{\beta}_0 \neq 0 \end{cases} \tag{35}$$

where  $\lambda_1 = \sqrt{(2 - K_1) K_2}$ . It can be concluded that  $u_{micropolar} = u_{Newtonian} = 1$  if  $\alpha_1 = 0$  with  $\tilde{\beta}_0 = 0$ .

(ii) The fluid speed  $u$  decreases with the rise in the micropolarity  $K_1$  because of the increase in the colloids of micropolar fluid.

(iii) The fluid speed  $u$  also decreases with the spin boundary condition parameter  $\tilde{\beta}_0$ .

### 4.2 Spin/Microrotation

Since there are no aciculate particles that collide in the Newtonian fluid ( $K_1 = 0$ ), the spin  $S = 0$  for it is as depicted in Fig. 4. The spin  $S$  lives with the micropolar fluid ( $K_1 \neq 0$ ) merely, and it controls the microrotation of aciculate particles as they collide about their centroids. Fig. 4 is plotted on the basis of Eq. (20). It shows that the spin  $S$  depends upon the micropolarity parameter  $K_1$ , the flow parameter  $\alpha_1$ , and the spin boundary parameter  $\tilde{\beta}_0$ . The dominance of rise in the spin is observed in the middle of the substrate because the spin of aciculate particles is linearly proportional to the velocity gradient.

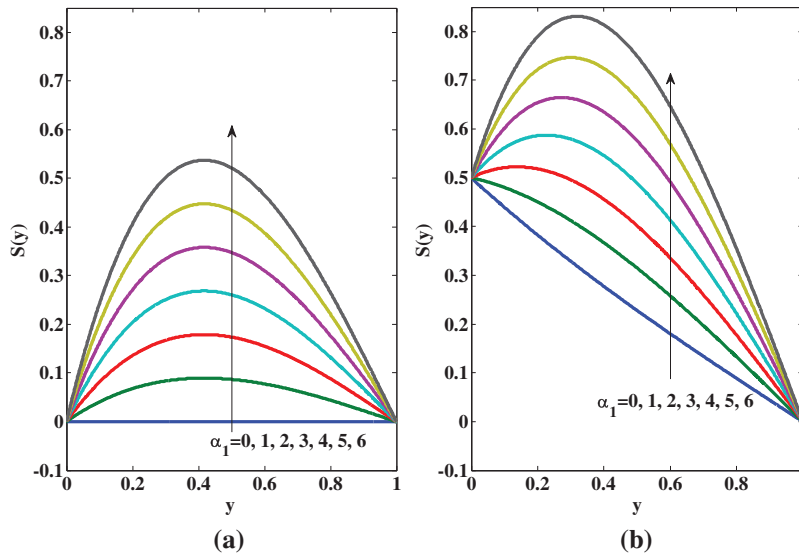


**Figure 4:** Variation of spin or microrotation of aciculate particles for micropolar fluid for different values of  $\alpha_1$  when  $K_1 = 1.5$  if spin coefficient: (a)  $\tilde{\beta}_0 = 0$ ; and (b)  $\tilde{\beta}_0 = 0.5$

Fig. 5 indicates that the spin rises with the micropolarity parameter  $K_1$  for all values of the flow parameter  $\alpha_1$  and spin boundary parameter  $\tilde{\beta}_0$ . Further, the spin is also enhanced with the spin

boundary parameter  $\tilde{\beta}_0$ . The increase in the spin is also observed as the flow parameter  $\alpha_1$  increases for all values of the spin boundary parameter  $\tilde{\beta}_0$  and micropolarity parameter  $K_1$ .

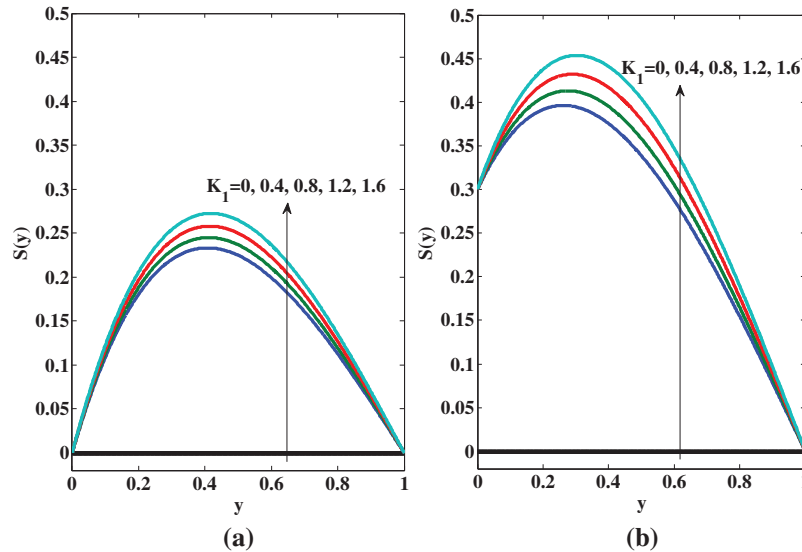


**Figure 5:** Variation of spin for micropolar fluid for different values of  $K_1$  when  $\alpha_1 = 3$  if spin coefficient: (a)  $\tilde{\beta}_0 = 0$ ; and (b)  $\tilde{\beta}_0 = 0.3$

### 4.3 Temperature

According to Eq. (21), the temperature  $\theta(y)$  majorly depends upon the flow parameter  $\alpha_1$ , the micropolarity parameter  $K_1$ , the viscous dissipation parameter  $\beta_3$ , and the spin boundary parameter  $\tilde{\beta}_0$  for the micropolar fluid. The variation of the temperature with respect to the aforementioned parameters is depicted in Fig. 6. Fig. 6c is plotted for comparison purposes for the Newtonian fluid ( $K_1 = 0$ ). The following can be derived when  $K_1 = 0$  is substituted in Eq. (21):

$$\frac{\theta(y)}{\beta_1} \Big|_{(K_1=0, \beta_3=0)} = \left[ -y + \frac{y^2}{2} + \left( \frac{1}{3}y - \frac{1}{6}y^3 + \frac{1}{24}y^4 \right) \alpha_1 \right] \beta_1 \tag{36}$$

Eq. (36) and Fig. 6c both align with Eq. (12) and Fig. 3a of [10]. Figs. 6a and 6b are plotted for micropolar fluid. These figures show that (i) the temperature increases across the channel as the micropolarity increases, due to the collides in the fluid, the thermal flux rises; (ii) the temperature for micropolar fluid is greater than the temperature for the Newtonian fluid consistently by the increase in the kinetic energy of the aciculate particles in the micropolar fluid; (iii) the temperature  $\theta$  increases with spin boundary parameter  $\tilde{\beta}_0$  because spin boundary condition reduces the thermal transfer rate; (iv) in contrast, the temperature  $\theta$  decreases with flow parameter  $\alpha_1$  for both micropolar and Newtonian fluids as it is expected due to the rise in the gravitational force; (v)  $\theta|_{Micropolar} = \theta|_{Newtonian} = \beta_1 \left[ \frac{y^2}{2} - y \right]$  for  $\alpha_1 = 0$  with  $\tilde{\beta}_0 = 0 = \beta_3$  for all points of the channel; (vi) If  $\alpha_1 = 0$  with  $\tilde{\beta}_0 \neq 0, \beta_3 \neq 0$  then the expression for temperature for micropolar fluid will differ slightly as:

$$\begin{aligned}
 4\theta(y, \alpha_1 = 0) = & -2(y - 2) \left\{ 2\beta_1 - \frac{K_1^2 \tilde{\beta}_0^2 \beta_3}{\sinh^2[\lambda_1]} \right\} - \frac{4yK_1 \tilde{\beta}_0 \beta_1}{\lambda_1} \\
 & - \frac{2K_1^2 \tilde{\beta}_0^2 \beta_3}{(-1 + e^{2\lambda_1})^2 \lambda_1} \{1 + e^{4\lambda_1} - e^{-2(y-2)\lambda_1} - e^{2y\lambda_1}\} \\
 & + \frac{2(\coth[\lambda_1] - 1) K_1 \tilde{\beta}_0 \beta_1}{\lambda_1^3} \{-1 + e^{2\lambda_1} - e^{-(y-2)\lambda_1} + e^{y\lambda_1} - 2y\lambda_1 e^{\lambda_1}\} \\
 & + \frac{2(\coth[\lambda_1] - 1) K_1 \tilde{\beta}_0 \beta_1}{2\lambda_1^3} \{1 - 2y^2\lambda_1^2 + e^{2y\lambda_1}(-1 + 2y\lambda_1)\}
 \end{aligned} \tag{37}$$

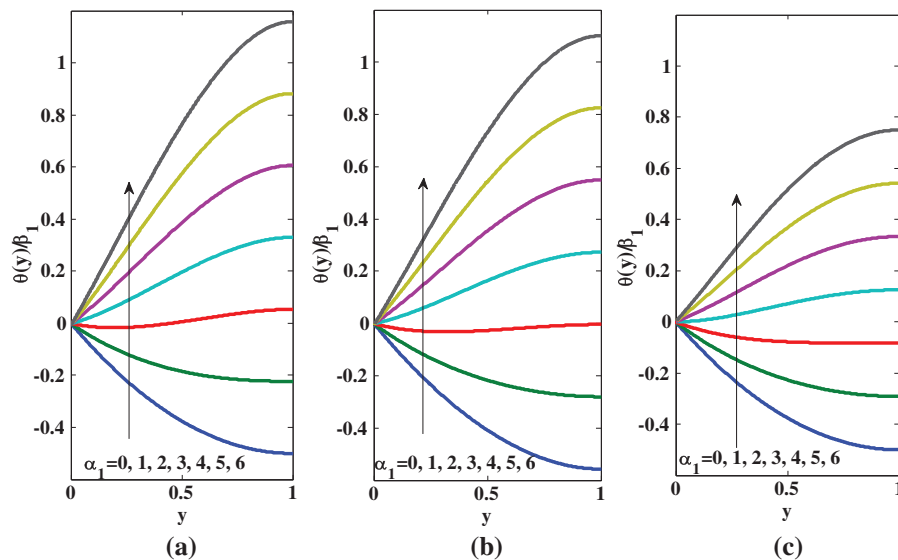


**Figure 6:** Temperature profile for different values of  $a_1$  when  $K_1 = 0.2$ ,  $\beta_3 = 0.0005$  for: (a) micropolar fluid, with zero spin boundary condition,  $\tilde{\beta}_0 = 0$ ; (b) micropolar fluid, with non-zero Spin boundary condition,  $\tilde{\beta}_0 = 0.5$ ; (c) Newtonian fluid

The variation of temperature at the air-nano micropolar fluid interface is important technoscientifically. It is examined by focusing on variation of  $\theta(1)$ . Its influence on flow and thermal parameters is presented in [Table 3](#) quantitatively, while respective expressions are given in [Table 2](#).

**Table 3:** Viscous dissipation  $\beta_3$  affects the temperature for different values of  $K_1$  and  $\tilde{\beta}_0$  when  $a_1 = 3$

$\tilde{\beta}_0$	$\beta_3$	$K_1$	$\theta(1)$
0	0	0.0	0.1250
		0.5	0.7701
		0.9	1.8442
	0.001	0.0	0.1243
		0.5	0.7673
		0.9	1.8365

(Continued)

**Table 3 (continued)**

$\tilde{\beta}_0$	$\beta_3$	$K_1$	$\theta$ (1)
0.5	0	0.0	0.1250
		0.5	0.6609
		0.9	1.6228
	0.001	0.0	0.1243
		0.5	0.6585
		0.9	1.6163

These tables show clearly the comparison between micropolar and Newtonian fluids. Table 3 depicts that the temperature  $\theta$  (1) at air-liquid interface increases as the micropolarity effect  $K_1$  of the micropolar fluid rises for all values of fluid and geometric parameters namely  $\beta_3$  and  $\tilde{\beta}_0$ .

The thermal transfer rate is significant in engineering and technology. It is studied in terms of the Nusselt number  $Nu$ , which is defined as [10]:

$$Nu = 2 \frac{\int_0^1 u dy}{\int_0^1 u \theta dy} \left( \frac{d\theta}{dy} \right)_{y=0} \tag{38}$$

If Eqs. (19)–(21) are substituted in Eq. (38), then one yields

$$Nu = \frac{R_0 R_1}{R_2} \tag{39}$$

where

$$R_0 = \frac{2}{3} \left( 3 - A_3 + \frac{6e^{\lambda_1} A_2 K_1 (-\text{Sinh}[\lambda_1] + \text{Cosh}[\lambda_1] \lambda_1)}{\lambda_1^2} \right) \tag{40a}$$

$$R_1 = \frac{1}{3\lambda_1^2} \left( -3(-1 - 2e^{2\lambda_1} + e^{4\lambda_1}) A_2^2 K_1^2 \beta_3 \lambda_1^2 + ((-3 + A_3) \beta_1 - A_3^2 \beta_3) \lambda_1^2 \right. \\ \left. + 3A_2 K_1 \left( (-1 + e^{\lambda_1}) \beta_1 (1 + e^{\lambda_1} (-1 + \lambda_1) + \lambda_1) \right) \right. \\ \left. + 2e^{2\lambda_1} A_3 \beta_3 (\text{Sinh}[\lambda_1] - \text{Cosh}[\lambda_1] \lambda_1) \right) \tag{40b}$$

$$R_2 = \frac{1}{5040\lambda_1^6} \left( -16((105 + A_3(-84 + 17A_3)) \beta_1 + (21 - 8A_3) A_3^2 \beta_3) \lambda_1^6 \right. \\ \left. + 840e^{3\lambda_1} A_2^3 K_1^3 \beta_3 \lambda_1^2 \left( \frac{24\text{Sinh}[\lambda_1]}{\lambda_1} \left( -24\text{Cosh}[\lambda_1] - 9\text{Sinh}[\lambda_1] + 7\text{Sinh}[3\lambda_1] \right) \right. \right. \\ \left. \left. + 4\text{Cosh}[\lambda_1] \lambda_1 (-3\text{Cosh}[2\lambda_1] + 2\lambda_1) \right) \right) \\ \left. + 7A_2^2 K_1^2 \lambda_1 \left( 20\beta_1 \left( \frac{77 + 63\lambda_1 - 12\lambda_1^3 + 36e^{\lambda_1}(-4 + \lambda_1^2) + 6e^{2\lambda_1}(30 - 3\lambda_1 + \lambda_1^3)}{+9e^{4\lambda_1}(7 - 9\lambda_1 + 2\lambda_1^3)7 + 4e^{3\lambda_1}(-44 + 3\lambda_1(8 + 3\lambda_1))} \right) \right. \right. \\ \left. \left. + 3\beta_3 \left( \frac{40e^{2\lambda_1} \lambda_1^3 (3\text{Sinh}[2\lambda_1] - 6\text{Cosh}[2\lambda_1] \lambda_1 + 4\lambda_1^2)}{+A_3 \left( -900e^{\lambda_1} (-1 + e^{4\lambda_1}) + \lambda_1 \left( \frac{-15 + 15e^{3\lambda_1} (128 + \text{Cosh}[\lambda_1] + 112\text{Cosh}[2\lambda_1] + \text{Sinh}[\lambda_1])}{+30(1 - 8e^{\lambda_1} + e^{4\lambda_1} + 8e^{5\lambda_1}) \lambda_1} \right) \right) \right) \right) \right) \right) \tag{40c}$$

$$+ 21A_2K_1 \left( \begin{array}{l} 20\beta_1\lambda_1^2 \left( \frac{21 + 21\lambda_1 - 8\lambda_1^3 + 12e^{\lambda_1}(-2 + \lambda_1^2)}{+e^{2\lambda_1}(3 - 3\lambda_1 + 2\lambda_1^3)} \right) \\ + 16A_3^2\beta_3 \left( \begin{array}{l} -15(-1 + e^{\lambda_1})(1 + e^{\lambda_1})(2 + 5e^{\lambda_1}) \\ + \lambda_1 \left( \begin{array}{l} 15(2 + 5e^{\lambda_1})(1 + e^{2\lambda_1}) \\ + \lambda_1 \left( \begin{array}{l} 15 + 5\lambda_1 - \lambda_1^3 + 5e^{3\lambda_1}(-3 + \lambda_1)(1 + \lambda_1) \\ -5e^{\lambda_1}(-1 + \lambda_1)(3 + \lambda_1) - e^{2\lambda_1}(15 - 5\lambda_1 + \lambda_1^3) \end{array} \right) \end{array} \right) \end{array} \right) \\ + A_3 \left( \begin{array}{l} 240e^{\lambda_1}\beta_3\lambda_1^2(3 + 3\lambda_1 + \lambda_1^2 - e^{2\lambda_1}(3 + (-3 + \lambda_1)\lambda_1)) \\ + \beta_1 \left( \begin{array}{l} 450 + 435\lambda_1 - 140\lambda_1^3 + 64\lambda_1^5 \\ -20e^{\lambda_1}(24 - 12\lambda_1^2 + 5\lambda_1^4) \\ -3e^{2\lambda_1}(-10 + \lambda_1(5 + 2\lambda_1(5 - 5\lambda_1 + 3\lambda_1^3))) \end{array} \right) \end{array} \right) \end{array} \right) \quad (41)$$

$$A_2 = \frac{\tilde{\beta}_0 + 2A_3}{e^{2\lambda_1} - 1} \quad (42a)$$

$$A_3 = \frac{2\alpha_1}{2 - K_1} \quad (42b)$$

The results related to the Nusselt number are shown quantitatively in Table 4 while qualitatively in Fig. 7a. Through Table 4 and Fig. 7a, it is observed that  $Nu$  depends upon the flow parameter  $\alpha_1$  significantly. It varies in three intervals or stages.  $Nu = 6$  is an initial value when  $\alpha_1 = 0$ , which is in agreement with the literature [72] for the Newtonian fluid ( $K_1 = 0$ ). It can be seen that the commencing value of  $Nu = 6$  for micropolar fluids for all values of  $K_1$  and shown in Fig. 7b. Its justification is that:  $R_0$ ,  $R_1$ , and  $R_2$  given as above equations, at  $\alpha_1 = 0$  are identical for Newtonian and micropolar fluids. Afterward, the Nusselt number rises till its amplitude (a couple of sample data are presented in Table 4). This peak value of  $Nu$  varies with the micropolarity effects. In the second stage,  $Nu$  decays strictly till a critical value of  $\alpha_1$ . This critical point varies with the micropolarity, as shown in Fig. 7. Finally, the Nusselt number increases monotonically till  $\alpha_1 \rightarrow \infty$ .

**Table 4:** Study of optimum/amplitude of the Nusselt number

$\tilde{\beta}_0$	$\beta_3$	$K_1$	$\alpha_1$	$(Nu)_{max}$	
0	0	0.0	2.333	20	
		0.04	2.264	17.4118	
		0.08	2.184	15.1364	
	0.001	0.0	2.34	20.0001	
		0.04	2.269	17.4533	
		0.08	2.188	15.2271	
	0.5	0	0.0	2.333	20
			0.04	2.269	18.0532
			0.08	2.199	16.3111
0.001		0.0	2.34	20.0001	
		0.04	2.273	18.0805	
		0.08	2.2	16.3712	

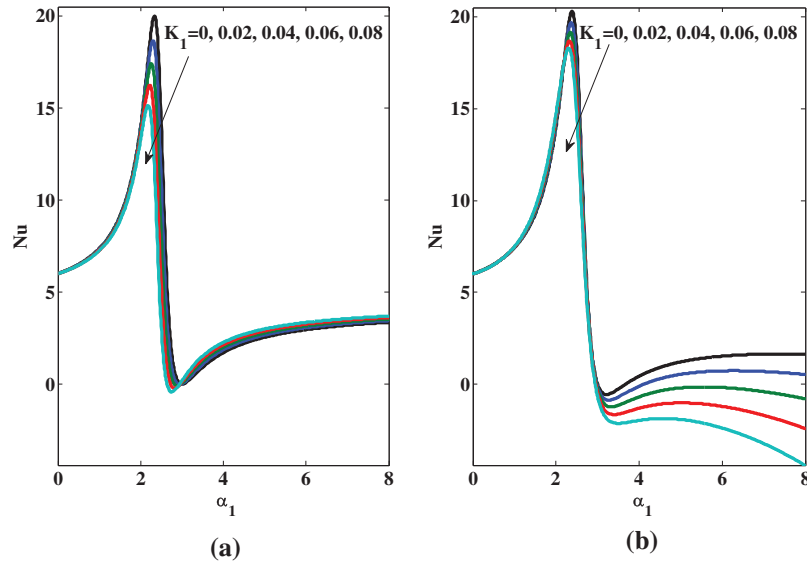


**Figure 7:** Variation of the Nusselt number  $Nu$  with flow parameter  $\alpha_1$  f  $\tilde{\beta}_0 = 0.001$  when: (a) without viscous dissipation  $\beta_3 = 0$ ; (b) with viscous dissipation  $\beta_3 = 0.2$ . Note that  $K_1 = 0$  represents the Newtonian fluid

#### 4.4 Influence of Nanoparticles

Let us define the following two important ratios to highlight the influences of nanoparticles [10]:

$$v_r = \frac{\mu_{nf} \rho_f}{\rho_{nf} \mu_f} \text{ and } k_r = \frac{k_{nf}}{k_f}. \tag{43}$$

There are five different types of samples of nanoparticles in order to examine in this current study, namely gold  $Au$ , silver  $Ag$ , molybdenum disulfide  $MoS_2$ , aluminum oxide  $Al_2O_3$ , and silicon dioxide  $SiO_2$  with a common base fluid in the blood, which is a micropolar fluid. The variation of relative viscosity  $v_r$  and relative thermal conductivity  $k_r$  with respect to the concentration of nanoparticles  $\varphi$  for both Newtonian and a micropolar fluids, respectively, are displayed in Figs. 8 and 9. Almost analogous trend is observed for both the fluids but a decrease in  $v_r$  and an increase in  $k_r$  are significant for a micropolar fluid. Furthermore, the gold and silver nanoparticles intensify in the flow parameter whereas the molybdenum disulfide, the aluminum oxide, and the silicon dioxide do decline in contribution in the flow parameter with the increase in the concentration of nanoparticles because  $v_r$  relays on the kinematics viscosity of the medium for both the Newtonian and the micropolar fluids as shown in Figs. 8a and 9a. Moreover, the enhancement in thermal transfer rate due to the presence of nanoparticles is physically expected, as demonstrated in Figs. 8b and 9b for both micropolar and Newtonian fluids. Notably, gold and silver achieve a higher transfer rate compared to molybdenum disulfide, aluminum oxide, and silicon dioxide due to their thermal conductivity in both base fluids (micropolar/Newtonian). Another significant observation concerns the influence of nanoparticles on film thickness during flow on an inclined substrate, as the film thickness is inversely proportional to the relative viscosity [10]. The reduction in film thickness in a nano-liquid containing gold particles, as compared to other nanoparticles, is noticeable due to the higher density or kinematic viscosity.

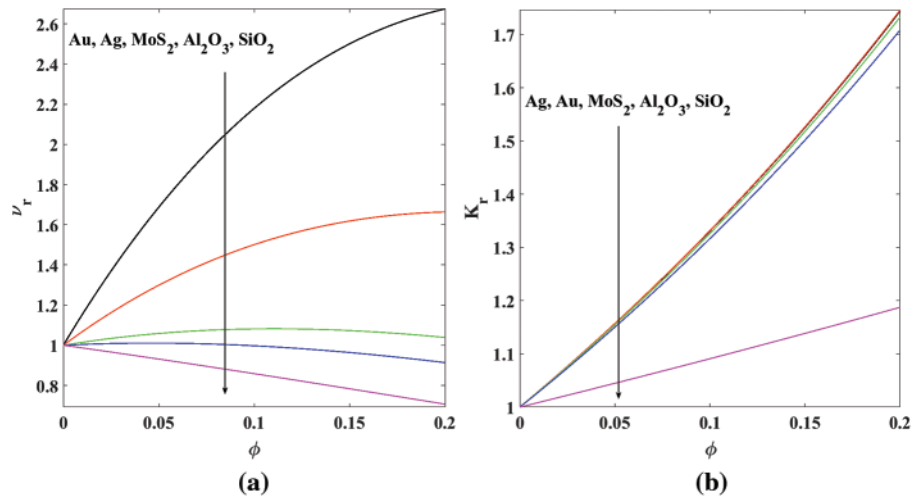


**Figure 8:** Effects of the concentration of nanoparticles  $\phi$  on: (a) flow parameter  $\nu_r$ ; (b) thermal parameter  $K_r$ , for the Newtonian fluid (pure water) as a base fluid

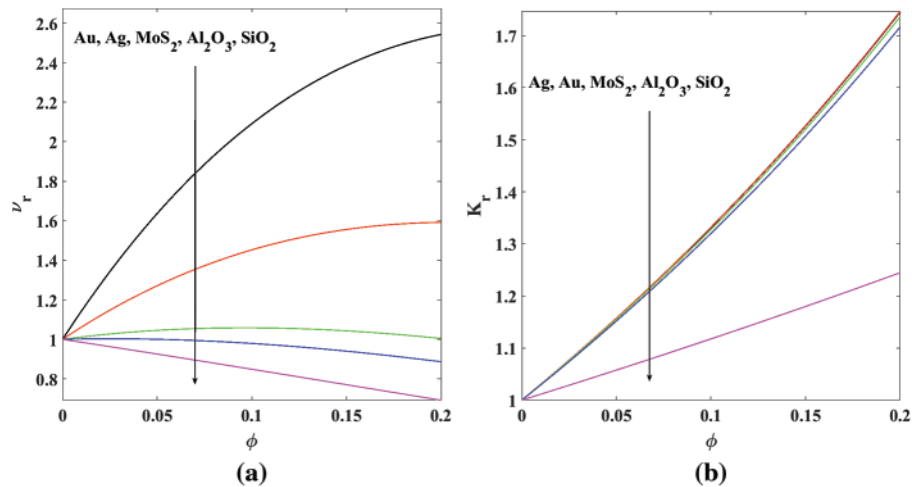


**Figure 9:** Effects of the concentration of nanoparticles  $\phi$  on: (a) flow parameter  $\nu_r$ ; (b) thermal parameter  $K_r$ , for the micropolar fluid (blood) as a base fluid

The concentration of nanoparticles  $\phi$  also affects the fluid speed and temperature. The fluid-speed  $u$  versus the concentration of the nanoparticles  $\phi$  at the middle of the channel is examined, and sample results are displayed in Figs. 10a and 10b for Newtonian and micropolar fluids as base liquids, respectively. Consistently, an almost similar trend is observed on  $u_{mid}$  for both fluids. However, the quantitative decay of  $u_{mid}$  for a micropolar fluid is compared to a Newtonian one for all test nanoparticles. The temperature at the middle of the channel  $\theta_{mid}$  exhibits analogous behavior to  $u_{mid}$ , as shown in Fig. 11.

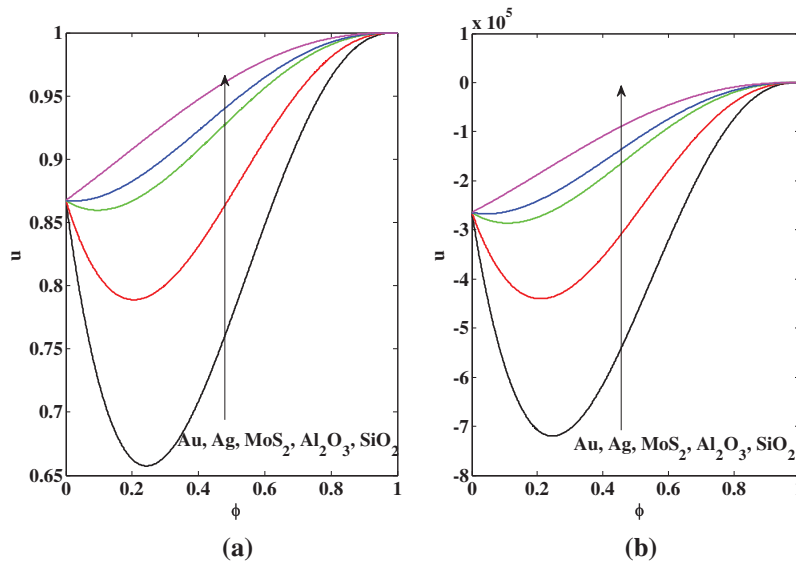


**Figure 10:** Midpoint channel effects of the concentration of nanoparticles  $\phi$  on fluid speed  $u$  if  $\tilde{\beta}_0 = 0.5$  for the base fluid as: (a) the Micropolar fluid (blood); (b) the Newtonian fluid (water)

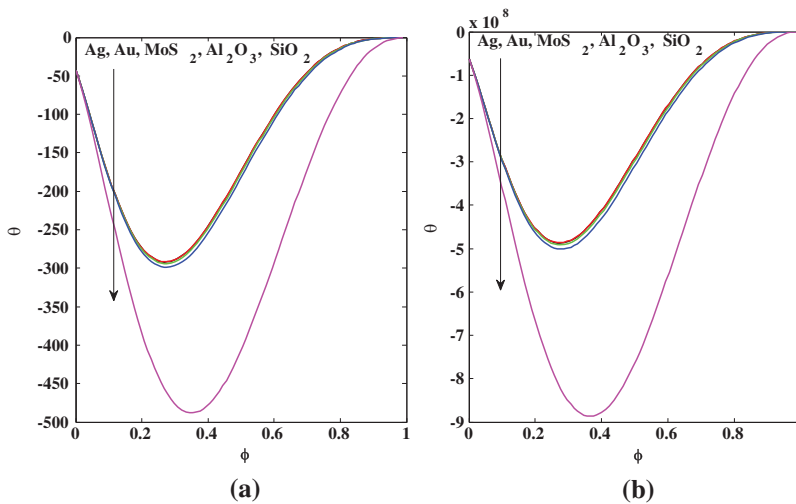


**Figure 11:** Midpoint channel effects of the concentration of nanoparticles  $\phi$  on temperature  $\theta$  for the base fluid as: (a) the Micropolar fluid (blood); (b) the Newtonian fluid (water)

### 5 Conclusion

In this study, the thin film flow of a micropolar fluid containing nanoparticles over an inclined substrate under the influence of viscous dissipation and gravitational force was formulated and examined theoretically. An exact solution to the formulated boundary value problem was derived for the first time. The variation of physical quantities, fluid speed, temperature, and microrotation/spin was analyzed based on the solution. The results are displayed in graphical and tabular form and compared to existing results from the literature for the Newtonian fluid as a particular case of the current study.

The results showed that the fluid velocity declines with increasing values of spin boundary condition and micropolarity due to the increase in colloids in the micropolar medium. Additionally, micropolarity with spin leads to an enhanced temperature field compared to a Newtonian fluid. Furthermore, it is observed that the Nusselt number rises until it reaches an amplitude that varies with micropolarity effects. Mid velocities eventually reveal a quantitative decay in a micropolar fluid compared to a Newtonian one for all tested nanoparticles, with similar behavior in temperature at the mid-channel. Gold and silver nanoparticles (i) intensify the flow parameters as the concentration of nanoparticles increases (ii) yield a higher thermal transfer rate, whereas molybdenum disulfide, aluminum oxide, and silicon dioxide exhibit the opposite behavior; this holds true for both Newtonian and micropolar fluids. Moreover, a reduction in film thickness for nano-liquid-containing gold particles, compared to other nanoparticles, is observed. Finally, it is important to state that this work is new and original.

**Acknowledgement:** The authors are extremely grateful to the editor of the journal and all four reviewers for very useful comments and suggestions.

**Funding Statement:** The authors did not receive any funding support from any source. It is self-financed solely.

**Author Contributions:** AAS: Conceptualization, Modeling, Calculations, Writing, Software; MT: Potential review, Keen validation, Proof reading, Collection of useful data, Valuable suggestions.

**Availability of Data and Materials:** MatLab was used to simulate the results. Upon reasonable request.

**Conflicts of Interest:** The authors have no conflict of interest to report regarding the present study.

## References

1. Bertozzi AL, Pugh M. The lubrication approximation for thin viscous films: regularity and long-time behavior of weak solutions. *Commun Pure Appl Math.* 1996 Feb;49(2):85–123. doi:10.1002/(ISSN)1097-0312.
2. Roy RV, Roberts AJ, Simpson ME. A lubrication model of coating flows over a curved substrate in space. *J Fluid Mech.* 2002 Mar;454:235–61. doi:10.1017/S0022112001007133.
3. Dutta A, Som SK, Das PK. Film condensation of saturated vapor over horizontal noncircular tubes with progressively increasing radius of curvature drawn in the direction of gravity. *J Heat Transfer.* 2004 Dec 1;126(6):906–14. doi:10.1115/1.1798891.
4. Taherzadeh D. Mechanics and substrate transport of moving biofilm structures (Ph.D. Thesis). Technische Universität München: Germany; 2011.
5. Howell PD, Robinson J, Stone HA. Gravity-driven thin-film flow on a flexible substrate. *J Fluid Mech.* 2013 Oct;732:190–213. doi:10.1017/jfm.2013.404.
6. Liu Y, Itoh M, Kyotoh H. Flow of a falling liquid curtain onto a moving substrate. *Fluid Dyn Res.* 2017 Jul 27;49(5):055501. doi:10.1088/1873-7005/aa7ee8.
7. Girtan M. Future solar energy devices. In: SpringerBriefs in applied sciences and technology. Cham: Springer; 2018. p. 1–104. doi:10.1007/978-3-319-67337-0.
8. Thiele U. Recent advances in and future challenges for mesoscopic hydrodynamic modelling of complex wetting. *Colloids Surf A: Physicochem Eng Asp.* 2018 Sep 20;553:487–95. doi:10.1016/j.colsurfa.2018.05.049.
9. Kreder MJ, Daniel D, Tetreault A, Cao Z, Lemaire B, Timonen JV, et al. Film dynamics and lubricant depletion by droplets moving on lubricated surfaces. *Phys Rev X.* 2018 Sep 4;8(3):031053.

10. Turkyilmazoglu M. Nanoliquid film flow due to a moving substrate and heat transfer. *Eur Phys J Plus*. 2020 Oct 6;135(10):781. doi:10.1140/epjp/s13360-020-00812-y.
11. Girtan M. On the electrical and photoelectrical properties of  $\text{CH}_3\text{NH}_3\text{PBI}_3$  perovskites thin films. *Sol Energy*. 2020 Jan 1;195:446–53. doi:10.1016/j.solener.2019.11.096.
12. Halpern D, Grotberg JB. Fluid-elastic instabilities of liquid-lined flexible tubes. *J Fluid Mech*. 1992 Nov;244:615–32. doi:10.1017/S0022112092003227.
13. Heil M, White JP. Airway closure: surface-tension-driven non-axisymmetric instabilities of liquid-lined elastic rings. *J Fluid Mech*. 2002 Jul;462:79–109. doi:10.1017/S0022112002008613.
14. Qayyum M, Ismail F, Sohail M, Imran N, Askar S, Park C. Numerical exploration of thin film flow of MHD pseudo-plastic fluid in fractional space: utilization of fractional calculus approach. *Open Phys*. 2021 Nov 26;19(1):710–21. doi:10.1515/phys-2021-0081.
15. Adesanya SO, Onanaye AS, Adeyemi OG, Rahimi-Gorji M, Alarifi IM. Evaluation of heat irreversibility in couple stress falling liquid films along heated inclined substrate. *J Clean Prod*. 2019 Dec 1;239:117608. doi:10.1016/j.jclepro.2019.117608.
16. Waini I, Ishak A, Pop I. Radiative and magnetohydrodynamic micropolar hybrid nanofluid flow over a shrinking sheet with Joule heating and viscous dissipation effects. *Neural Comput Appl*. 2022 Mar;34(5):3783–94. doi:10.1007/s00521-021-06640-0.
17. Bilal M, Ramzan M, Siddique I, Sajjad A. Magneto-micropolar nanofluid flow through the convective permeable channel using Koo-Kleinstreuer–Li model. *J Magn Magn Mater*. 2023 Jan 1;565:170288. doi:10.1016/j.jmmm.2022.170288.
18. Rajkumar D, Reddy AS, Narayana PS, Jagadeshkumar K, Chamkha AJ. Pulsating magnetohydrodynamic flow of  $\text{Fe}_3\text{O}_4$ -blood based micropolar nanofluid between two vertical porous walls with Cattaneo-Christov heat flux and entropy generation. *J Magn Magn Mater*. 2023 Apr 1;571:170564. doi:10.1016/j.jmmm.2023.170564.
19. Bayareh M. An overview of non-Newtonian nanofluid flow in macro-and micro-channels using two-phase schemes. *Eng Anal Bound Elem*. 2023 Mar 1;148:165–75. doi:10.1016/j.enganabound.2022.12.033.
20. Nabwey HA, Rahbar F, Armaghani T, Rashad AM, Chamkha AJ. A comprehensive review of non-newtonian nanofluid heat transfer. *Symmetry*. 2023 Jan 29;15(2):362. doi:10.3390/sym15020362.
21. Siddiqui AA, Lakhtakia A. Steady electro-osmotic flow of a micropolar fluid in a microchannel. *Proc R Soc A: Math, Phys Eng Sci*. 2009 Feb 8;465(2102):501–22. doi:10.1098/rspa.2008.0354.
22. Siddiqui AA, Turkyilmazoglu M. Slit flow and thermal analysis of micropolar fluids in a symmetric channel with dynamic and permeable. *Int Commun Heat Mass Transf*. 2022 Mar 1;132:105844. doi:10.1016/j.icheatmasstransfer.2021.105844.
23. Nusselt W. Die oberflächenkondensation des wasserdampfes. *VDI-Zs*. 1916;60:541.
24. Tamir A, Taitel Y. Nusselt condensation with interfacial resistance. *Chem Eng J*. 1974 Jan 1;7(3):245–7. doi:10.1016/0300-9467(74)85038-0.
25. Kondic L, Diez J. Pattern formation in the flow of thin films down an incline: constant flux configuration. *Phys Fluids*. 2001 Nov 1;13(11):3168–84. doi:10.1063/1.1409965.
26. O'Brien SBG, Schwartz LW. Theory and modeling of thin film flows. 2002. Available from: <https://api.semanticscholar.org/CorpusID:11512995>. [Accessed 2023].
27. Wang H, Rose JW. Film condensation in horizontal microchannels: effect of channel shape. *Int Conf Nanochannels, Microchannels, Minichannels*. 2005 Jan 1;41855:729–35.
28. Al-Jarrah JA, Khadrawi AF, Al-Nimr MA. Film condensation on a vertical microchannel. *Int Commun Heat Mass Transf*. 2008 Nov 1;35(9):1172–6. doi:10.1016/j.icheatmasstransfer.2008.07.003.
29. Gatapova EY, Kabov OA. Shear-driven flows of locally heated liquid films. *Int J Heat Mass Transf*. 2008 Sep 1;51(19–20):4797–810.

30. Lin TS, Kondic L, Filippov A. Thin films flowing down inverted substrates: three-dimensional flow. *Phys Fluids*. 2012;24:022105. doi:10.1063/1.3682001.
31. Mazloomi A, Moosavi A. Thin liquid film flow over substrates with two topographical features. *Phys Rev E*. 2013 Feb 26;87(2):022409. doi:10.1103/PhysRevE.87.022409.
32. Slade DR. Gravity-driven thin liquid films: rivulets and flow dynamics. England, UK: University of Leeds; 2013.
33. Ju W, Wu Y, Lin S, Zhao F, Tan S. Visual experimental study of droplet impinging on liquid film and analysis of droplet evolution characteristics. *Exp Comput Multiph Flow*. 2022;4(3):212–20. doi:10.1007/s42757-020-0081-3.
34. Charogiannis A, Markides CN. Spatiotemporally resolved heat transfer measurements in falling liquid-films by simultaneous application of planar laser-induced fluorescence (PLIF), particle tracking velocimetry (PTV) and infrared (IR) thermography. *Exp Therm Fluid Sci*. 2019 Oct 1;107:169–91. doi:10.1016/j.expthermflusci.2018.11.001.
35. Wang XF, Hrnjak PS, Elbel S, Jacobi AM, He MG. Heat transfer performance for a falling-film on horizontal flat tubes. *J Heat Transf*. 2013 Jul 1;135(7):072901. doi:10.1115/1.4023689.
36. Budakli M. Hydrodynamics and heat transfer in gas-driven liquid film flows (Ph.D. Thesis). Institute of Technical Thermodynamics, Technische Universitat Darmstadt: Germany; 2015.
37. Markides CN, Mathie R, Charogiannis A. An experimental study of spatiotemporally resolved heat transfer in thin liquid-film flows falling over an inclined heated foil. *Int J Heat Mass Transf*. 2016 Feb 1;93:872–88. doi:10.1016/j.ijheatmasstransfer.2015.10.062.
38. Miladinova S, Lebon G, Toshev E. Thin-film flow of a power-law liquid falling down an inclined plate. *J Non-Newton Fluid Mech*. 2004 Sep 20;122(1–3):69–78.
39. Siddiqui AM, Mahmood R, Ghori QK. Some exact solutions for the thin film flow of a PTT fluid. *Phys Lett A*. 2006 Aug 14;356(4–5):353–6.
40. Siddiqui AM, Mahmood R, Ghori QK. Homotopy perturbation method for thin film flow of a fourth grade fluid down a vertical cylinder. *Phys Lett A*. 2006 Apr 3;352(4–5):404–10.
41. Siddiqui AM, Mahmood R, Ghori QK. Homotopy perturbation method for thin film flow of a third grade fluid down an inclined plane. *Chaos, Solitons Fractals*. 2008 Jan 1;35(1):140–7. doi:10.1016/j.chaos.2006.05.026.
42. Alam MK, Siddiqui AM, Rahim MT, Islam S, Avital EJ, Williams JJ. Thin film flow of magnetohydrodynamic (MHD) pseudo-plastic fluid on vertical wall. *Appl Math Comput*. 2014 Oct 15;245:544–56.
43. Singh J, Kumar D, Baleanu D. A hybrid analytical algorithm for thin film flow problem occurring in non-Newtonian fluid mechanics. *Ain Shams Eng J*. 2021 Jun 1;12(2):2297–302. doi:10.1016/j.asej.2020.09.006.
44. Tlili I, Samrat SP, Sandeep N, Nabwey HA. Effect of nanoparticle shape on unsteady liquid film flow of MHD Oldroyd-B ferrofluid. *Ain Shams Eng J*. 2021 Mar 1;12(1):935–41. doi:10.1016/j.asej.2020.06.007.
45. Abdal S, Siddique I, Salamat N, Ud Din IS. Nano-bio-film flow of Williamson fluid due to a non-linearly extending/contracting surface with non-uniform physical properties. *Waves Random Complex Media*. 2022 Nov 16;1–9. doi:10.1080/17455030.2022.2146233.
46. Alali E, Megahed AM. MHD dissipative Casson nanofluid liquid film flow due to an unsteady stretching sheet with radiation influence and slip velocity phenomenon. *Nanotechnol Rev*. 2022 Jan 15;11(1):463–72. doi:10.1515/ntrev-2022-0031.
47. Esmaeili E, Grassia P, Ulloa CAT. Squeeze film flow of viscoplastic Bingham fluid between non-parallel plates. *J Non-Newton Fluid Mech*. 2022 Jul 1;305:104817. doi:10.1016/j.jnnfm.2022.104817.
48. Qayyum M, Ismail F, Ali Shah SI, Sohail M, El-Zahar ER, Gokul KC. An application of homotopy perturbation method to fractional-order thin film flow of the Johnson-Segalman fluid model. *Math Probl Eng*. 2022 Feb 23;2022:1–7.

49. Hassan MH, Al-Saif AS. A mathematical model for the velocity of thin film flow of a third grade fluid down in an inclined plane. *J Adv Res Fluid Mech Therm Sci*. 2023 Feb 13;102(1):140–52. doi:10.37934/arfmts.
50. Ashraf H, Sabir S, Siddiqui AM, Rehman HU, Almutairi B, Shah NA. Heat transfer analysis of temperature dependent viscosity Johnson-Segalman fluid film flow on a vertical heated belt. *Case Stud Therm Eng*. 2023 Sep 1;49:103362. doi:10.1016/j.csite.2023.103362.
51. Mahesh T, Panda S. Longwave modeling of thin film flow of a generalized second-grade fluid down a slanted plate. *Int J Non Linear Mech*. 2023 Mar 1;149:104327. doi:10.1016/j.ijnonlinmec.2022.104327.
52. Mandal S, Shit GC. Entropy analysis of unsteady magnetohydrodynamic thin liquid film flow of Maxwell nanofluids with variable fluid properties. *Mater Chem Phys*. 2023 Jan 1;293:126890. doi:10.1016/j.matchemphys.2022.126890.
53. Vanitha GP, Shobha KC, Mallikarjun BP, Mahabaleshwar US, Bognár G. Casson nanoliquid film flow over an unsteady moving surface with time-varying stretching velocity. *Sci Rep*. 2023 Mar 11;13(1):4074. doi:10.1038/s41598-023-30886-4.
54. Turk MA, Sylvester ND, Ariman T. On pulsatile blood flow. *Trans Soc Rheol*. 1973 Mar 1;17(1):1–21. doi:10.1122/1.549295.
55. Misra JC, Ghosh SK. A mathematical model for the study of interstitial fluid movement vis-a-vis the non-Newtonian behaviour of blood in a constricted artery. *Comput Math Appl*. 2001 Mar 1;41(5–6):783–811.
56. Eringen AC. *Microcontinuum field theories: II. fluent media*. London, UK: Springer Science & Business Media; 2001 Mar 30.
57. Papautsky I, Brazzle J, Ameel T, Frazier AB. Laminar fluid behavior in microchannels using micropolar fluid theory. *Sens Actuators A: Phys*. 1999 Mar 9;73(1–2):101–8.
58. Yusuf TA, Kumar RN, Prasannakumara BC, Adesanya SO. Irreversibility analysis in micropolar fluid film along an incline porous substrate with slip effects. *Int Commun Heat Mass Transf*. 2021 Jul 1;126:105357. doi:10.1016/j.icheatmasstransfer.2021.105357.
59. Ahmad S, Naveed Khan M, Ali R, Ahmad Lone S. Analysis of free bioconvective flow of hybrid nanofluid induced by convectively heated cone with entropy generation. *Mod Phys Lett B*. 2024 Jan 30;38(03):2450015. doi:10.1142/S0217984924500155.
60. Ali L, Ali B, Iqbal T. Finite element analysis of the impact of particles aggregation on the thermal conductivity of nanofluid under chemical reaction. *Waves Random Complex Media*. 2023 Feb 4;1–21.
61. Shah SA, Ahammad NA, Ali B, Guedri K, Awan AU, Gamaoun F, et al. Significance of bio-convection, MHD, thermal radiation and activation energy across Prandtl nanofluid flow: a case of stretching cylinder. *Int Commun Heat Mass Transf*. 2022 Oct 1;137:106299. doi:10.1016/j.icheatmasstransfer.2022.106299.
62. Abbas N, Rehman KU, Shatanawi W, Abodayeh K. Mathematical model of temperature-dependent flow of power-law nanofluid over a variable stretching Riga sheet. *Waves Random Complex Media*. 2022 Aug 18;1–8. doi:10.1080/17455030.2022.2111029.
63. Stfytkora D, Kašička V, Mikšík I, Řezanka P, Záruba K, Matějka P, et al. Application of gold nanoparticles in separation sciences. *J. Sep. Sci*. 2010 Feb;33(3):372–87. doi:10.1002/jssc.v33:3.
64. Cabuzu D, Cirja A, Puiu R, Mihai Grumezescu A. Biomedical applications of gold nanoparticles. *Curr Top Med Chem*. 2015 Aug 1;15(16):1605–13. doi:10.2174/1568026615666150414144750.
65. Zaaroura I, Harmand S, Carlier J, Toubal M, Fasquelle A, Nongaillard B. Thermal performance of self-wetting gold nanofluids: application to two-phase heat transfer devices. *Int J Heat Mass Transf*. 2021 Aug 1;174:121322. doi:10.1016/j.ijheatmasstransfer.2021.121322.
66. Hao D, Yang R, Yi N, Cheng H. Highly sensitive piezoresistive pressure sensors based on laser-induced graphene with molybdenum disulfide nanoparticles. *Sci China Technol Sci*. 2021 Nov;64(11):2408–14. doi:10.1007/s11431-021-1899-9.

67. Luo SW, Alimujiang A, Cui J, Chen TT, Balamurugan S, Zheng JW, et al. Molybdenum disulfide nanoparticles concurrently stimulated biomass and  $\beta$ -carotene accumulation in *Dunaliella salina*. *Bioresour Technol*. 2021 Jan 1;320:124391. doi:10.1016/j.biortech.2020.124391.
68. Gudkov SV, Burmistrov DE, Smirnova VV, Semenova AA, Lisitsyn AB. A mini review of antibacterial properties of  $\text{Al}_2\text{O}_3$  nanoparticles. *Nanomater*. 2022 Jul 30;12(15):2635. doi:10.3390/nano12152635.
69. Wei J, He C, Lv G, Zhuang Y, Qian Y, Pan S. The combustion, performance and emissions investigation of a dual-fuel diesel engine using silicon dioxide nanoparticle additives to methanol. *Energy*. 2021 Sep 1;230:120734. doi:10.1016/j.energy.2021.120734.
70. Shuai C, Yang F, Shuai Y, Peng S, Chen S, Deng Y, et al. Silicon dioxide nanoparticles decorated on graphene oxide nanosheets and their application in poly(l-lactic acid) scaffold. *J Adv Res*. 2023 Jun 1;48:175–90. doi:10.1016/j.jare.2022.08.017.
71. Nield DA, Kuznetsov AV. Forced convection in a parallel-plate channel occupied by a nanofluid or a porous medium saturated by a nanofluid. *Int J Heat Mass Transf*. 2014 Mar 1;70:430–3. doi:10.1016/j.ijheatmasstransfer.2013.11.016.
72. Ilyas SU, Pendyala R, Marneni N. Stability of nanofluids. In: *Engineering applications of nanotechnology: from energy to drug delivery*. Springer International Publishing; 2017. p. 1–31.
73. Khan MR, Puneeth V, Alqahtani AM, Alhazmi SE, Beinane SA, Shutaywi M, et al. Numerical simulation and mathematical modeling for heat and mass transfer in MHD stagnation point flow of nanofluid consisting of entropy generation. *Sci Rep*. 2023 Apr 19;13(1):6423. doi:10.1038/s41598-023-33412-8.